

Absorbing aerosol choices influence precipitation changes across future scenarios

Isabel L. McCoy^{1,2}, Mika Vogt³, and Robert Wood³

¹Rosenstiel School of Marine and Atmospheric Science, University of Miami, Miami, FL, 33149-1031, USA

²Cooperative Programs for the Advancement of Earth System Science, University Corporation for Atmospheric Research, Boulder, CO, 80307-3000, USA

³Department of Atmospheric Sciences, University of Washington, Seattle, WA, 98195-1640, USA

Key Points:

- Atmospheric energy budgets are used to constrain absorbing aerosol influences on 21st century precipitation in ScenarioMIP projections.
- Shared socioeconomic pathways with aerosol cleanup policies can significantly augment 21st century global precipitation.
- Impacts of regional aerosol changes on precipitation are equal or larger than the influence from atmospheric circulation changes.

15 **Abstract**

16 Future precipitation changes are controlled by the atmospheric energy budget, with tem-
 17 perature, water vapor, and absorbing aerosols playing dominant roles in driving radia-
 18 tive changes. Atmospheric energy budgets are calculated for different Shared Socioeco-
 19 nomic Pathways (SSPs) using ScenarioMIP projections from phase 6 of the Climate Model
 20 Intercomparison Project and are used to quantify the influence of 21st century aerosol
 21 cleanup on precipitation. Absorbing aerosol influences on shortwave absorption are iso-
 22 lated from the effects of water vapor. Apparent hydrologic sensitivity is ~40% higher
 23 for the *Middle of the Road* (SSP2-4.5) scenario with aerosol cleanup than for the *Regional*
 24 *Rivalry* (SSP3-7.0) scenario that maintains aerosol. Regionally, cleanup-induced changes
 25 in the atmospheric energy budget are of a similar magnitude to the precipitation increases
 26 themselves and are larger than the influence of changes in atmospheric circulation. Pol-
 27 icy choices about future absorbing aerosol emissions will therefore have major impacts
 28 on global and regional precipitation changes.

29 **Plain Language Summary**

30 Precipitation changes will have a temperature-dependent and a temperature-independent
 31 part of their response to climate change. Water vapor contributes primarily to the for-
 32 mer while well-mixed greenhouse gases will influence both. The temperature-independent
 33 response will be impacted by absorbing aerosol emissions. This is examined through an
 34 atmospheric energy budget where precipitation (i.e., latent heat) balances other energy
 35 sources and sinks in the atmosphere (i.e., sensible heat, shortwave and longwave radi-
 36 ration). We utilize a novel set of global climate model simulations that incorporate var-
 37 ied socioeconomic choices over the 21st century to study real-world implications of fu-
 38 ture aerosol policies on precipitation. Reductions in absorbing aerosol amount help pre-
 39 cipitation to increase because less shortwave absorption will occur in the atmosphere and,
 40 on average, other energy contributions do not change per degree warming. Global pre-
 41 cipitation change per degree of global warming is ~40% higher for socioeconomic path-
 42 ways where aerosol cleanup occurs. Regional precipitation changes associated with re-
 43 gional aerosol changes are larger than those associated with changes in atmospheric cir-
 44 culation. Policy choices for aerosol emissions will thus have a critical impact on the fu-
 45 ture availability of water, both globally and regionally.

46 **1 Introduction**

47 Regional and global changes in precipitation are expected over the 21st century driven
 48 by increasing greenhouse gases, changes in aerosols, and changes in land use (Allan et
 49 al., 2020). These factors influence precipitation by changing atmospheric longwave emis-
 50 sion, shortwave absorption, and surface sensible heat fluxes (Pendergrass & Hartmann,
 51 2014; Allan et al., 2020). A major fraction of the inter-model variance in global mean
 52 precipitation increase has been shown to be associated with uncertainties in clear sky
 53 shortwave absorption (Pendergrass & Hartmann, 2012; DeAngelis et al., 2015), changes
 54 in which are controlled primarily by water vapor path (WVP) and absorbing aerosols.

55 Emissions of aerosols over the 21st century are expected to change markedly, with
 56 changes strongly dependent upon socioeconomic pathways (Lund et al., 2019). WVP in-
 57 creases with global mean temperature, closely following Clausius-Clapeyron (C-C) scal-
 58 ing of ~7% K⁻¹ (Held & Soden, 2006; Allan et al., 2014). Precipitation increases much
 59 more slowly with temperature (Held & Soden, 2006) and is constrained by the atmospheric
 60 energy budget (Pendergrass & Hartmann, 2014).

61 Precipitation changes can be separated into temperature-dependent and temperature-
 62 independent responses (M. R. Allen & Ingram, 2002; Andrews et al., 2010). WVP con-
 63 tributes primarily to the former as it is strongly tied to temperature. Some aerosols (e.g.,

sulfate) contribute to the temperature-dependent response through scattering sunlight back to space, cooling the surface (Allan et al., 2020). Absorbing aerosols (e.g., black carbon) influence precipitation mostly through the temperature-independent response (Richardson et al., 2018; Allan et al., 2020). Although well-mixed greenhouse gases (WMGHGs) mainly drive the temperature-dependent response, they also contribute to the fast, temperature-independent precipitation response (Richardson et al., 2018).

Climate drivers that significantly influence precipitation through the fast response (e.g., WMGHGs, absorbing aerosols) do so by affecting the atmospheric energy budget. In particular, absorbing aerosols change the amount of shortwave radiation absorbed by the atmosphere and that can impact the surface sensible heat flux. There are other mechanisms by which aerosols are thought to impact precipitation as well. An increase in aerosol amount can lead to a shift from lighter to heavier rain rates and, in the case of absorbing aerosols, a suppression of small clouds and promotion of deeper clouds through increasing instability and convective inhibition. Aerosols are also known to impact circulation patterns, which will influence regional precipitation (Allan et al., 2020). In order to reduce uncertainties in projected precipitation, it is important to understand the role that aerosols play in the poorly-constrained temperature-independent response (Allan et al., 2020). In this study, we focus on understanding how different aerosol policy choices effect precipitation through the fast response.

In the most recent Coupled Model Intercomparison Project (CMIP6), models ran scenarios designated by Shared Socioeconomic Pathways (SSPs) — representing possible policies over the next century — and 2100 forcing levels in W m^{-2} (Eyring et al., 2016). Different policies strongly influence absorbing aerosol changes, impacting future precipitation through the temperature-independent response. These ScenarioMIP simulations (described in Section 2) allow an examination of how policy decisions can influence different aspects of future climate.

We use an atmospheric energy budget framework to estimate contributions from projected changes in absorbing aerosols to changes in global and regional precipitation. We focus especially on two scenarios, SSP2-4.5 and SSP3-7.0, as they offer a contrasting aerosol strategy (cleanup vs. no cleanup, respectively) at intermediate radiative forcing pathways. Section 2 describes the models and methods. Global and regional precipitation change results are presented in Sections 3 and 4, respectively. Section 5 presents a comparison of different methods to constrain the contribution of changes in absorbing aerosols to the precipitation response across scenarios.

2 Materials and Methods

2.1 CMIP6 ScenarioMIP Simulations

We examine climate model projections from four Tier-1 ScenarioMIP scenarios from CMIP6. Each scenario has a distinct SSP and a different level of forcing following the Representative Concentration Pathways (RCPs) used in previous CMIPs (Neill et al., 2016; Riahi et al., 2017). The SSPs factor in differences in societal development related to societal concerns around climate change. Lower SSPs (e.g., SSP1: *Sustainability*, SSP2: *Middle of the Road*) have fewer challenges to climate mitigation and adaptation while higher SSPs have more (e.g., SSP3: *Regional Rivalry*, SSP5: *Fossil-fueled Development*) (Riahi et al., 2017).

SSP1-2.6 uses the RCP2.6 pathway, is the most weakly-forced scenario considered (experiencing less than 2°C warming by 2100 in the multi-model mean), and undergoes substantial land-use change. SSP2-4.5 undergoes intermediate forcing, is an update to RCP4.5, and has less extreme changes in aerosol and land use compared to other SSPs. SSP3-7.0 has a higher forcing (an update to RCP7.0). In particular, it has large land use changes and maintains high emissions of short lived climate forcers (e.g., aerosols) un-

114 til 2100. Finally, SSP5-8.5 is the most strongly-forced scenario considered, an update to
 115 RCP8.5.

116 Our analysis focuses on changes between the present day (2015-2025) and the end
 117 of this century (2090-2100) using composites from 18 CMIP6 models (Table S1). Results
 118 are largely insensitive to the length of the averaging period over the range 10-20 years.
 119 We have chosen to utilize the 10-year averaging periods in order to leverage the longest
 120 record possible from the CMIP6 simulations and thus examine the largest change from
 121 the present climate. All currently available models with outputs necessary for estimat-
 122 ing absorbing aerosol contributions to the atmospheric energy budget are included, with
 123 absorbing aerosol optical depth at 550nm wavelength (*AAOD*) used to describe absorb-
 124 ing aerosol amount. Global changes in key quantities for the four scenarios are listed in
 125 Table S2 while trends in CO₂ and WVP and their correspondence are shown in Fig. S1.
 126

127 The 21st century trend in *AAOD*, which is primarily driven by changes in black
 128 carbon emissions, varies strongly across the four scenarios (Fig. 1a). Strong *AAOD* re-
 129 ductions in SSP1-2.6, SSP2-4.5 reflect aggressive aerosol cleanup policies, weaker reduc-
 130 tions occur in SSP5-8.5, and SSP3-7.0 is distinguished by having no *AAOD* reductions
 131 over this period (Turnock et al., 2020). There is larger inter-model variability for *AAOD*
 132 than for the other CMIP6 variables we examine. Some of this is associated with uncer-
 133 tainty in the present-day aerosol state. SSP multi-model mean trends in the anomaly
 134 of *AAOD* from the 2015-2025 period are distinct (Fig. S2a). SSP1-2.6, SSP2-4.5, and
 135 SSP5-8.5 models agree on the sign of the global mean $\Delta AAOD$ at 90% confidence ($\sim 16/18$
 136 models, Fig. S2b). All CMIP6 models produce a small, near-zero global mean $\Delta AAOD$
 137 for SSP3-7.0 and all model behaviors are distinctly separated from the contrasting SSP2-
 138 4.5 case.

139 All mean and standard error (SE) values from the budget and other calculations
 140 are listed in the supplemental tables, S2-S5. Where relevant, mean $\pm 2SE$ values are re-
 141 ported in the text to facilitate comparisons at 95% confidence.

142 2.2 Absorbing aerosol impacts on the atmospheric energy budget

143 To quantify the impact of absorbing aerosol changes on precipitation, we adopt an
 144 atmospheric energy budget approach (e.g., Pendergrass and Hartmann (2014)). Glob-
 145 ally, precipitation change (ΔP) reflects change in atmospheric latent heating (ΔLH),
 146 which, together with atmospheric sensible heating (ΔSH), must be balanced by reduc-
 147 tions in absorbed energy in the net atmospheric longwave (ΔLW) and shortwave (ΔSW):

$$-L_v \Delta P = -\Delta LH = \Delta SH + \Delta SW + \Delta LW \quad (1)$$

148 where L_v is the latent heat of vaporization. Water vapor and absorbing aerosol changes
 149 dominate ΔSW (Richardson et al., 2018). We use a multiple regression to separate these
 150 contributions. For each scenario, global annual multi-model mean time series of *WVP*,
 151 *AAOD* and net *SW* are constructed. The resulting fit, parabolic in ΔWVP and linear
 152 in $\Delta AAOD$, explains 99.8% of the variance of ΔSW at 95% confidence (Fig. S3):

$$\Delta SW = a \cdot \Delta WVP + b \cdot (\Delta WVP)^2 + c \cdot \Delta AAOD \quad (2)$$

153 where $a = 0.693 \pm 0.009 \text{ W kg}^{-1}$, $b = -0.016 \pm 0.001 \text{ W kg}^{-2} \text{ m}^2$, and $c = 520 \pm 9 \text{ W m}^{-2}$,
 154 with errors providing 95% confidence intervals. We note that c , which is computed for
 155 all models together, is within the standard error of the multi-model mean atmospheric
 156 absorption dependence on *AAOD* found in CMIP5 AeroCom models, $525 \pm 92 \text{ W m}^{-2}$
 157 (see Table 3 in Myhre et al., 2013). The quadratic term in ΔWVP is needed to account
 158 for the sub-linear dependency of solar absorption on *WVP* (Lacis & Hansen, 1974) but
 159 is relatively weak, contributing only 5-15% of the overall ΔWVP contribution to *SW*
 160 absorption.

161 3 Changes in Global Precipitation over the 21st century

162 Within each scenario (i.e., for fixed radiative forcing), global mean precipitation
 163 ΔP increases at $\sim 2.5\%$ per degree of global mean warming (Fig. 1b) consistent with $2\text{--}3\% \text{ K}^{-1}$
 164 in earlier studies (Samset et al., 2018). Although this slope (i.e., the hydrologic
 165 sensitivity, η), is consistent across SSPs (Table S2), the intercepts of the ensemble mem-
 166 ber fits differ significantly. The SSP differences in response can also be described by the
 167 apparent hydrologic sensitivity, $\eta_a = L_v \Delta P / \Delta T$ (Allan et al., 2020), using the multi-
 168 model means (Table S2). SSP3-7.0 stands out as it has a substantially lower ΔP than
 169 would be expected from the ΔT experienced in this scenario ($1.30 \pm 0.14 \text{ W m}^{-2} \text{ K}^{-1}$).
 170 Indeed, instead of falling between SSP2-4.5 (1.76 ± 0.14) and SSP5-8.5 (1.39 ± 0.14),
 171 the SSP3-7.0 line nearly overlaps the SSP5-8.5 line (Fig. 1b).

172 To explore this further, Fig. 1c shows multi-model mean changes in the atmospheric
 173 budget terms for the four scenarios (Table S2). As ΔT increases, all terms correspond-
 174 ingly increase in magnitude. Negative ΔLW indicates increasing atmospheric radiative
 175 cooling as temperature increases (Pendergrass & Hartmann, 2014), which is remarkably
 176 linear in ΔT . In contrast, changes in ΔSW , ΔSH , and ΔLH ($\equiv L_v \Delta P$) all show devi-
 177 ations from linear behavior. Specifically, SSP3-7.0 has a markedly stronger increase in
 178 ΔSW ($3.51 \pm 0.34 \text{ W m}^{-2}$) and, as a result, a muted increase in ΔLH ($3.86 \pm 0.38 \text{ W m}^{-2}$)
 179 and thus precipitation at this ΔT ($3.00 \pm 0.30 \text{ K}$). The lack of deviation by ΔLW ($-6.24 \pm 0.62 \text{ W m}^{-2}$)
 180 in SSP3-7.0 suggests that anomalies in WMGHGs and WVP are unlikely to be driving
 181 the anomalous precipitation response in SSP3-7.0. Instead, ΔSW is likely a major driver
 182 of the unusual behavior seen in SSP3-7.0 ΔP (Fig. 1b, c). The lack of aerosol cleanup
 183 in this scenario (Fig. 1a) may be muting precipitation increases over the 21st century
 184 compared with scenarios that undergo cleanup.

185 We examine two scenarios in detail, SSP2-4.5 and SSP3-7.0, that represent inter-
 186 mediate RCP pathways in the ScenarioMIP simulations but with substantially different
 187 SSP aerosol emission choices. Using Eq. 2, we quantify the contributions of $\Delta AAOD$ (ΔSW_{AAOD})
 188 and ΔWVP (ΔSW_{WVP}) to ΔSW . These are shown along with the remaining energy
 189 budget terms from Eq. 1 in Fig. 2. To control for differences in forcing (i.e., tempera-
 190 ture change) between scenarios, energy budgets are examined per degree of global warm-
 191 ing and terms are reported as sensitivities (Table S3). The normalized precipitation change
 192 (i.e., apparent hydrologic sensitivity) is $\sim 40\%$ larger for SSP2-4.5 ($1.8 \pm 0.6 \text{ W m}^{-2} \text{ K}^{-1}$)
 193 than for SSP3-7.0 ($1.3 \pm 0.4 \text{ W m}^{-2} \text{ K}^{-1}$). ΔLW (-2.2 vs. $-2.1 \pm 0.6 \text{ W m}^{-2} \text{ K}^{-1}$) and
 194 ΔSW_{WVP} ($1.1 \pm 0.4 \text{ W m}^{-2} \text{ K}^{-1}$) sensitivities are remarkably similar between these
 195 scenarios, indicating they are not the primary drivers of differences in η_a . Instead, the
 196 difference in η_a can be explained by differences in absorbing aerosol pathways between
 197 the two scenarios, SSP2-4.5 (Fig. 2a) and SSP3-7.0 (Fig. 2b): ΔSW_{AAOD} is the major
 198 contributor to the difference (-0.50 ± 0.14 vs. $0.026 \pm 0.014 \text{ W m}^{-2} \text{ K}^{-1}$) but ΔSH also
 199 has a small contribution (-0.19 ± 0.06 vs. $-0.33 \pm 0.1 \text{ W m}^{-2} \text{ K}^{-1}$). Aerosol cleanup in
 200 SSP2-4.5 reduces SW absorption (0.64 ± 0.18 vs. $1.2 \pm 0.4 \text{ W m}^{-2} \text{ K}^{-1}$ for SSP3-7.0),
 201 offsetting approximately 60% of the increased SW absorption driven by increased WVP
 202 and increasing the amount of SW that can contribute to the surface SH . This results
 203 in a larger global precipitation increase in SSP2-4.5 while the lack of cleanup in SSP3-
 204 7.0 results in a muted 21st century precipitation increase.

205 4 Factors Influencing Regional Precipitation Changes

206 Given that aerosol cleanup choices can significantly effect global precipitation changes,
 207 we now explore the extent to which regional $\Delta AAOD$ is expected to influence regional
 208 precipitation over the 21st century. Geographic patterns of $\Delta AAOD$ are highly hetero-
 209 geneous. We focus on two regions with striking 21st century $\Delta AAOD$ (Table S4, Fig. S4),
 210 which are also thought to be dominated by the temperature-independent precipitation
 211 response (Samset et al., 2016): Southeastern Asia ($0\text{--}45^\circ\text{N}$, $60\text{--}130^\circ\text{E}$) and Equatorial

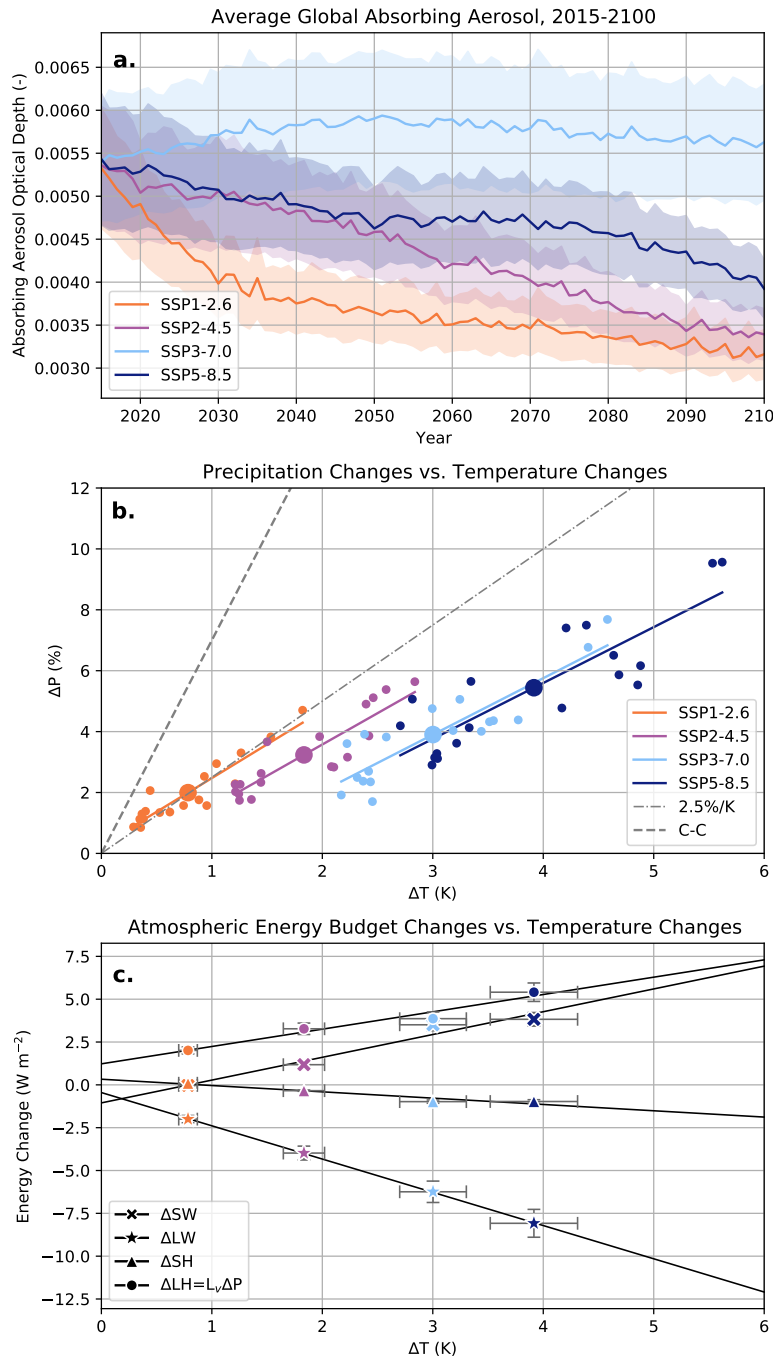


Figure 1. (a) Global multi-model ensemble mean (line) and corresponding standard error (shading) for *AAOD* by scenario across period of interest (2015-2100). Global mean changes in (b) precipitation and (c) atmospheric energy budget terms plotted as a function of global mean surface air temperature changes (Table S2). Changes are computed as the difference between two ten-year periods, 2090-2100 and 2015-2025. In (b), projections from each contributing model (small circles) and the scenario multi-model mean (large circles) are shown. The ratio of the ensemble mean $\Delta P / \Delta T$ represents the apparent hydrologic sensitivity. The slope of the best fit line through the individual ensemble members for each scenario represents the hydrologic sensitivity (Table S2), which is $\sim 2.5\% \text{ K}^{-1}$ for each scenario (dot-dash). The C-C response (i.e., $\sim 7\% \text{ K}^{-1}$) is included for reference (dash). In (c), one SE is used to indicate uncertainty in the multi-model mean budget terms while maintaining visual clarity.

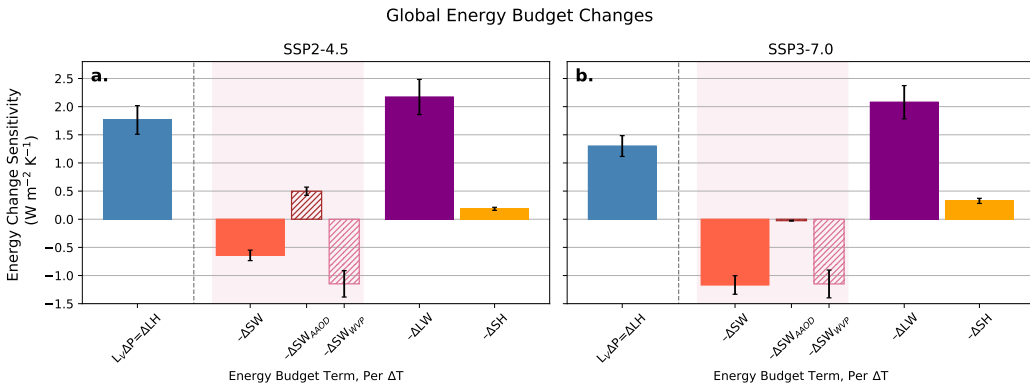


Figure 2. Global changes in the atmospheric energy budget (2015-2025 to 2090-2100) for two scenarios with contrasting aerosol choices: (a) SSP2-4.5 and (b) SSP3-7.0 (Table S3). Energy budget terms are normalized by the change in global mean surface air temperature and expressed as sensitivities. ΔSW (solid) is decomposed into two (hatched) components, ΔSW_{AAOD} and ΔSW_{WVP} , based on Eq. 2. Solid bars on the right of the dashed line sum to the precipitation change on the left following Eq. 1. Bars represent multi-model means while error bars represent 2SE based on the variability in the multi-model mean 10-year periods propagated through the change and normalization calculations. Standard errors for ΔSW components also include coefficient uncertainties.

Africa (15°S - 15°N , 30°W - 30°E). Strong aerosol cleanup occurs in both regions in SSP2-4.5 (-9.12 ± 0.98 and $-4.98 \pm 0.58 \cdot 10^{-3}$, respectively) with $\sim 90\%$ of models agreeing in the sign of the multi-model mean regional $\Delta AAOD$ (Fig. S5b, S6b). In SSP3-7.0, aerosol loadings increase in Equatorial Africa ($2.97 \pm 0.3 \cdot 10^{-3}$) and decrease slightly in SE Asia ($-1.74 \pm 0.36 \cdot 10^{-3}$). Although the $\Delta AAOD$ is smaller in this scenario, most models still agree in sign of the mean change over the region (Fig. S5c, S6c). The consistency across CMIP6 models in regional behavior for these SSPs supports our choice in selecting these areas to study.

The regions studied here are sufficiently large (>3000 km in scale) that atmospheric energy and water budgets are useful for assessment of their precipitation changes (Dagan et al., 2019a; Dagan & Stier, 2020). On a regional scale the energy and moisture budgets are:

$$L_v\Delta P = -\Delta SH - \Delta SW - \Delta LW + \Delta div(s) \quad (3)$$

$$\Delta P = \Delta E - \Delta div(q_v) = \Delta LH/L_v - \Delta div(q_v) \quad (4)$$

where $div(s)$ and $div(q_v)$ are residuals representing the divergences of dry static energy and column integrated moisture, respectively, reflecting the exports of energy and moisture required to balance the regional budgets.

Fig. 3 and Table S5 present contributions of each of the normalized terms in Eqns. 3 and 4 to the overall, normalized ΔP experienced in each region under SSP2-4.5 (4.0 ± 1.2 vs. $1.6 \pm 0.6 \text{ W m}^{-2} \text{ K}^{-1}$ in SE Asia vs. Equatorial Africa) and SSP3-7.0 (2.6 ± 0.8 vs. 1.3 ± 0.6). Examining the simpler water budget (Eq. 4) first, we find ΔLH sensitivity differs between SSPs but not regionally: SSP2-4.5 (2.8 vs. $2.7 \pm 0.8 \text{ W m}^{-2} \text{ K}^{-1}$ in SE Asia vs. Equatorial Africa) has a larger change than SSP3-7.0 (1.7 vs. 1.6 ± 0.4). However, $\Delta div(q_v)$ sensitivity varies more between regions than by SSP: SE Asia experiences increased moisture convergence (-1.1 ± 1.2 vs. $-0.9 \pm 0.8 \text{ W m}^{-2} \text{ K}^{-1}$ in SSP2-4.5 vs. SSP3-7.0) while Equatorial Africa experiences the opposite (1.2 ± 0.8 vs. 0.3 ± 0.6). The net result is a substantial variation between both region and scenario for regional η_a .



Figure 3. Regional atmospheric energy and moisture budget changes (2015–2025 to 2090–2100) for SSP2-4.5 (panels a, c) and SSP3-7.0 (panels b, d) for Southeast Asia ($0\text{--}45^\circ\text{N}$, $60\text{--}130^\circ\text{E}$; panels a, b) and Equatorial Africa ($15^\circ\text{S}\text{--}15^\circ\text{N}$, $30^\circ\text{W}\text{--}30^\circ\text{E}$; panels c, d) (Table S5). Budget term normalization, ΔSW decomposition, bar and error bar meanings as in Fig. 2. Normalized energy budget terms (solid bars between dashed lines) sum to the normalized precipitation change (left) following Eq. 3 while normalized water budget terms (solid bars to the right of dashed lines) sum following Eq. 4.

The regional energy budget provides insight into variability in regional η_a (Fig. 3). As in the global budget (Fig. 2), ΔLW (SE Asia: -2.4 ± 0.6 vs. $-2.6 \pm 0.8 \text{ W m}^{-2} 4 \text{ K}^{-1}$ in SSP2-4.5 vs. SSP3-7.0; Equatorial Africa: -2.7 vs. -2.5 ± 0.8) and ΔSW_{WVP} (SE Asia: 1.5 ± 0.8 for both; Equatorial Africa: 1.7 vs. 1.6 ± 1.0) variation across region and SSP is very small compared to other, more explicit differences between terms. WMGHGs and WVP may have more complex influences on the regional and inter-scenario differences in precipitation response, for example by affecting regional circulation patterns as discussed below. Instead, ΔSW_{AAOD} , ΔSH , and $\Delta div(s)$ differences appear to drive the majority of the variability in regional η_a .

Absorbing aerosol driven changes in SW absorption (ΔSW_{AAOD}) are the leading contributor to energy budget changes between the two scenarios in both regions as can be seen by comparing left versus right panels in Fig. 3 (SE Asia: -2.6 ± 0.8 vs. $-0.30 \pm 0.14 \text{ W m}^{-2} \text{ K}^{-1}$ in SSP2-4.5 vs. SSP3-7.0; Equatorial Africa: -1.4 ± 0.4 vs. 0.51 ± 0.14). The smaller contributions from ΔSH (SE Asia: 0.58 ± 0.18 vs. -0.11 ± 0.04 ; Equatorial Africa: 0.47 ± 0.16 vs. -0.14 ± 0.06), and $\Delta div(s)$ (SE Asia: 1.5 ± 1.2 vs. 1.0 ± 0.8 ; Equatorial Africa: -0.6 vs. 0.3 ± 0.8) may also be associated with aerosol changes through influencing SW availability at the surface and regional circulation patterns. Overall, this implies that a substantial fraction of the markedly higher regional η_a for SSP2-4.5 vs. SSP3-7.0 can be explained by aerosol cleanup policies. Note that this applies in both regions even though

257 aerosol loadings increased in SSP3-7.0 in Equatorial Africa while SE Asia experienced
 258 a smaller cleanup in SSP3-7.0 than in SSP2-4.5.

259 Aerosol forcing can impact circulation, and thus precipitation, changes in Equa-
 260 torial Africa through shifting the location of the inter-tropical convergence zone (R. J. Allen
 261 et al., 2015; Chemke & Dagan, 2018; Wang, 2015) and in SE Asia through changing the
 262 monsoon circulation (Bollasina et al., 2011). Increased AAOD in the tropics may influ-
 263 ence precipitation through thermally driven circulation changes from modification of $\text{div}(s)$
 264 (Dagan et al., 2019b, 2021) but absorbing aerosol perturbations over Equatorial Africa
 265 and SE Asia are expected to have a small effect (Dagan et al., 2021). Indeed, changes
 266 in both $\Delta\text{div}(s)$ and $\Delta\text{div}(q_v)$ sensitivity (SE Asia: -1.1 ± 1.2 vs. $-0.9 \pm 0.8 \text{ W m}^{-2} \text{ K}^{-1}$
 267 in SSP2-4.5 vs. SSP3-7.0; Equatorial Africa: 1.2 ± 0.8 vs. 0.3 ± 0.6) between scenar-
 268 os are considerably smaller than those in ΔSW_{AAOD} . This implies that regional pre-
 269 cipitation changes between scenarios are more strongly controlled by aerosol absorption
 270 changes than they are by changes in the import or export of energy and moisture, sug-
 271 gestive of a relatively small role for atmospheric circulation changes.

272 To better understand the circulation responses, we estimate the thermodynamic
 273 contribution to precipitation-evaporation ($P-E$) changes that would occur in the ab-
 274 sence of changes in the lower tropospheric circulation. Using Eq. 5, we estimate the mois-
 275 ture convergence $\Delta\text{div}(q_v)_{thermo}$ driven solely by increased WVP (Fig. 4) assuming the
 276 circulation remains fixed (i.e., Held and Soden (2006)):

$$\Delta(P - E) \approx \alpha(P - E)\Delta T = -\Delta\text{div}(q_v)_{thermo} \quad (5)$$

277 where E is evaporation and $\alpha \approx 0.07$. We use $\Delta\text{div}(q_v)_{thermo}$ in Eq. 4 to estimate a pre-
 278 dicted change in precipitation, ΔP_{thermo} , absent circulation changes. The difference, $\Delta P_{circ} =$
 279 $\Delta P - \Delta P_{thermo}$, is an estimate of the influence that circulation has on regional precip-
 280 itation. Similarly, the difference $\Delta\text{div}(q_v)_{circ} = \Delta\text{div}(q_v) - \Delta\text{div}(q_v)_{thermo}$ is an esti-
 281 mate of the circulation influence on regional moisture convergence changes.

282 Comparing the magnitude of the circulation change influence on precipitation (ΔP_{circ} ,
 283 SE Asia: -0.8 ± 1.6 vs. $-1.0 \pm 1.0 \text{ W m}^{-2} \text{ K}^{-1}$ in SSP2-4.5 vs. SSP3-7.0; Equatorial Africa:
 284 -0.6 ± 1.2 vs. 0.3 ± 0.8) to the magnitude of the AAOD influence on SW (ΔSW_{AAOD}),
 285 we conclude that the influence of aerosol cleanup (SSP2-4.5) has a larger influence on
 286 ΔP than do changes in circulation for both Equatorial Africa and SE Asia (Fig. 4 a, c,
 287 Tables S4, S5). When aerosol emissions follow a regional rivalry framework (SSP3-7.0),
 288 the influence of aerosol radiative changes is of an equivalent magnitude to circulation changes
 289 in Equatorial Africa (where aerosol increases) and is smaller than the circulation influ-
 290 ence in SE Asia (where aerosol still reduces but by a smaller magnitude than in SSP2-
 291 4.5) (Fig. 4 b, d, Tables S4, S5). Although circulation changes clearly influence regional
 292 precipitation trends over the 21st century on spatial scales of several thousand kilome-
 293 ters, such changes are unlikely to exceed those driven by local cleanup efforts in regions
 294 with high loadings of absorbing aerosol.

295 Our estimate of the influence of aerosol cleanup on regional precipitation is likely
 296 a lower bound. This is because we only explicitly account for the effect of aerosol changes
 297 on precipitation through SW absorption and have not separately estimated the circu-
 298 lation change resulting from the remote and local coupling to aerosol forcing that is ex-
 299 pected to influence these regions. However, our results do indicate that we should ex-
 300 pect that, through SW absorption, SH flux, and circulation changes, aerosol cleanup (in
 301 SSP2-4.5, compared with SSP3-7.0) will accelerate increases in precipitation in both re-
 302 gions examined.

303 5 Quantifying absorbing aerosol influences on precipitation

304 These atmospheric energy budget examinations provide compelling evidence that
 305 future choices in aerosol emissions will influence precipitation over the 21st century, both

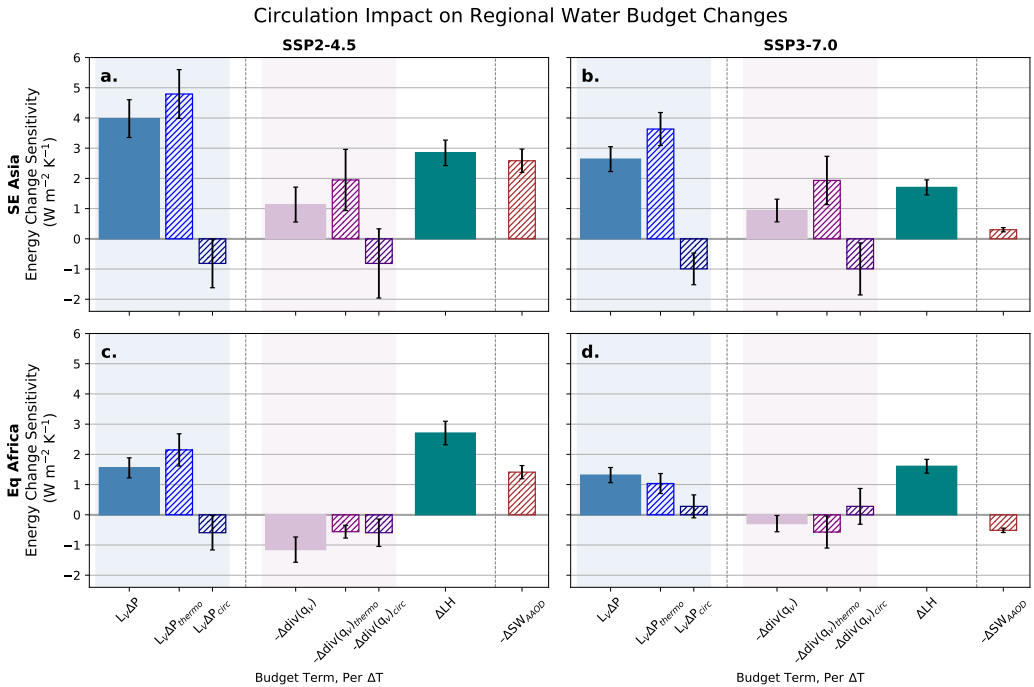


Figure 4. Estimation of regional changes in circulation (2015–2025 to 2090–2100) for SSP2-4.5 (a, c) and SSP3-7.0 (b, d) for Southeast Asia (a, b) and Equatorial Africa (c, d) (Table S5). Budget term normalization, bar and error bar meanings as in Fig. 3. Thermodynamic ($\Delta \text{div}(q_v)_{\text{thermo}}$, ΔP_{thermo}) and circulation ($\Delta \text{div}(q_v)_{\text{circ}}$, ΔP_{circ}) contributions to the total ($\Delta \text{div}(q_v)$, ΔP) are estimated using Eqns. 5 and 4. ΔSW_{AAOD} (Fig. 3), the only ΔSW component changing between regions and SSPs, is included for reference.

regionally and globally. Absorbing aerosol, via ΔSW , affects precipitation mostly through the fast (i.e., temperature-independent) response (M. R. Allen & Ingram, 2002). In this section, we quantify the fast response associated with $\Delta AAOD$ using three different analysis methods (Fig. 5, Table S2).

The first and simplest method uses multiple linear regression to establish temperature-dependent and AAOD-dependent influences on ΔP (Fig. 5a). This regression explains 86% of the variance in global ΔP across all SSPs at 95% confidence. Using the coefficient for the $\Delta AAOD$ contribution, we estimate the aerosol-driven portion of ΔP (ΔP_{AAOD}) for each scenario (Fig. 5b).

The second method follows Allan et al. (2020), producing an independent estimate of the fast response that does not use $\Delta AAOD$. We estimate the temperature-dependent precipitation response (η) and the combined temperature-dependent and independent response (η_a) from Fig. 1b (see Section 3). The fast precipitation response for SSPs is the difference between these hydrologic sensitivities:

$$\Delta P_{\text{fast}} = \Delta T (\eta - \eta_a). \quad (6)$$

Table S2 shows η , η_a , and ΔP_{fast} global estimates by scenario. We expect η to be scenario independent since it is a model-specific quantity and all SSP simulations use the same set of CMIP6 models. Indeed, individual SSP η 's are within uncertainties of each other. For consistency in our calculations, we use the scenario mean value for all

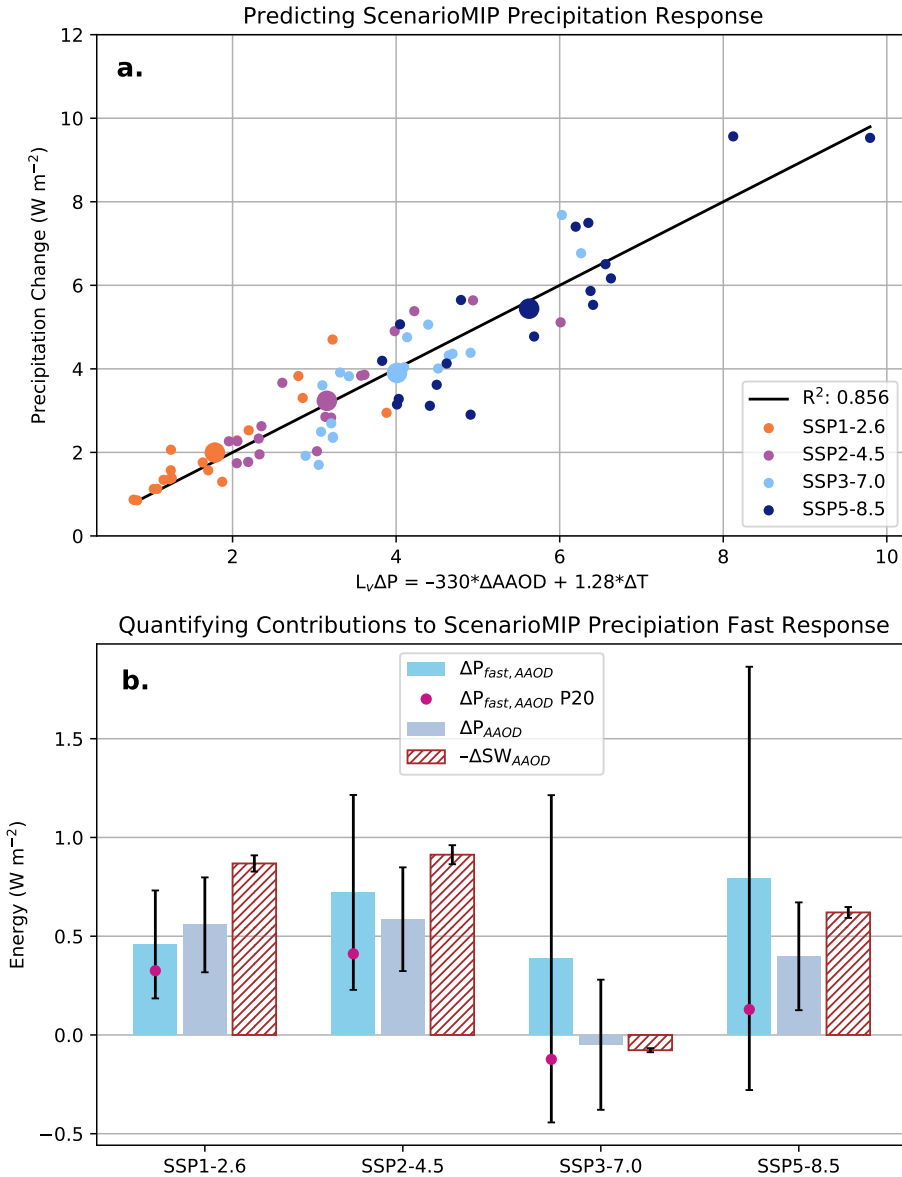


Figure 5. Quantifying the fast precipitation responses in ScenarioMIP simulations through various methods (Table S2). (a) A multiple linear regression on $\Delta AAOD$ and ΔT for global ensemble members across all SSPs explains 86% of the variance at 95% confidence of the total precipitation response, ΔP . (b) Using the relationship in (a), we estimate the AAOD contribution, ΔP_{AAOD} , and contrast it with estimates of $\Delta P_{fast,AAOD}$, explained in the text, and ΔSW_{AAOD} . The $\Delta P_{fast,AAOD}$ comparison (red circle) uses $\eta=2.16$ (Pendergrass, 2020) instead of $2.02 \text{ W m}^{-2} \text{ K}^{-1}$ (this study). All of these temperature-independent energy terms are significantly smaller for SSP3-7.0 than in the other SSPs, signifying the importance of $\Delta AAOD$ in determining ΔP . Bars represent multi-model mean and errors represent one SE instead of 2SE to account for large uncertainty in $\Delta P_{fast,AAOD}$ for SSP5-8.5.

324 SSPs, $\eta_{SSP} = 2.02 \pm 0.26 \text{ W m}^{-2} \text{ K}^{-1}$ (Table S2). This is within uncertainties of a multi-
 325 model mean estimate from abrupt 4xCO₂ CMIP6 simulations, $\eta = 2.16 \text{ W m}^{-2} \text{ K}^{-1}$ (Pendergrass,
 326 2020).

327 The fast response includes contributions from changes in absorbing aerosols as well
 328 as WMGHGs, most importantly ΔCO_2 and, to a lesser extent, ΔCH_4 and other WMGHG:

$$\Delta P_{fast} = \Delta P_{fast,AAOD} + \Delta P_{fast,CO2} + \Delta P_{fast,CH4} + \Delta P_{fast,other}. \quad (7)$$

329 To calculate $\Delta P_{fast,AAOD}$ for each scenario from Eq. 7, we use ΔP_{fast} estimates (Ta-
 330 ble S2) and assume $\Delta P_{fast,other}$ is negligible. We rely on Richardson et al. (2018)'s sen-
 331 sitivity studies to estimate fast precipitation responses for the two dominant WMGHGs
 332 (CO₂ and CH₄): a doubling of CO₂ has a -2.2 W m⁻² response while a tripling of CH₄
 333 has -0.5 W m⁻² (see their Fig. 1). Assuming contributions of CO₂ and CH₄ to the fast
 334 response depend logarithmically on concentration (consistent with Andrews et al. (2010)
 335 and Laakso et al. (2020)), we construct the following equations for fast responses from
 336 arbitrary gas concentration changes:

$$\begin{aligned} \Delta P_{fast,CO2} &= -\left(\frac{2.2}{\ln 2}\right) \ln\left(\frac{[CO_2^f]}{[CO_2^i]}\right) \\ \Delta P_{fast,CH4} &= -\left(\frac{0.5}{\ln 3}\right) \ln\left(\frac{[CH_4^f]}{[CH_4^i]}\right) \end{aligned} \quad (8)$$

337 Superscripts *i* and *f* in Eq. 8 indicate initial (2015-2025 mean) and final (2090-2100 mean)
 338 concentrations, respectively. [CO₂] and [CH₄] are the respective gas concentrations for
 339 CO₂ and CH₄ from Meinshausen et al. (2020). These contributions to ΔP_{fast} and the
 340 final $\Delta P_{fast,AAOD}$ (Fig. 5b) are listed in Table S2 by scenario. We also include an es-
 341 timate of $\Delta P_{fast,AAOD}$ in Fig. 5b using η from Pendergrass (2020) (P20) that falls within
 342 uncertainties, suggesting $\Delta P_{fast,AAOD}$ is not overly sensitive to our η determination.

343 The only other WMGHG that contributes significantly to the atmospheric energy
 344 budget is nitrous oxide (N₂O), but estimates of its impact on fast precipitation responses
 345 are not available in the literature. The TOA forcing from N₂O over the 21st century is
 346 estimated to be less than 0.3 W m⁻² for all SSPs studied here (Meinshausen et al., 2020).
 347 Assuming the fast precipitation response from N₂O scales similarly with TOA forcing
 348 as for other WMGHG (CO₂ and CH₄), then $\Delta P_{fast,N2O}$ would range from -0.05 W m⁻²
 349 in SSP1-2.6 to -0.13 W m⁻² in SSP3-7.0. The small range and magnitude of these es-
 350 timated responses, and the significant statistical uncertainties in the estimates of ΔP_{fast}
 351 (Table S2), justifies our choice to exclude the effects of N₂O from our estimates of $\Delta P_{fast,AAOD}$.

352 The third method relies on the idea that changes in atmospheric SW absorption
 353 from aerosol (ΔSW_{AAOD}) translate into precipitation changes in the absence of changes
 354 in the other energy budget terms (ΔSH , ΔLW , and ΔSW_{WVP}). This neglects the in-
 355 fluence that an increase in SW absorption associated with an increase in absorbing aerosol
 356 will have on the SH flux through reducing the amount of SW that reaches the surface,
 357 a much smaller effect (Fig. 2). Since the relative changes in these other terms are small
 358 across scenarios (Figs. 1, 2, Table S2), ΔSW_{AAOD} is an approximate estimate of the global
 359 ΔP due to absorbing aerosol changes (Fig. 5b).

360 Despite the large uncertainty in the residual estimation of $\Delta P_{fast,AAOD}$, we find
 361 relatively good agreement across scenarios between $\Delta P_{fast,AAOD}$ and ΔP_{AAOD} deter-
 362 mined from regressing ΔP against ΔT and $\Delta AAOD$ (Fig. 5b). All methods agree that
 363 SSP3-7.0 has a precipitation response to AAOD that is very small compared with other
 364 scenarios, consistent with little global aerosol cleanup (Fig. 1a). The variation of pre-
 365 cipitation response to $\Delta AAOD$ across scenarios is also consistent with our independent
 366 expectations from the atmospheric energy budget, as shown by reductions in shortwave
 367 absorption by aerosol ($\Delta SW_{AAOD} < 0$) over the 21st century in all scenarios except SSP3-
 368 7.0 (Fig. 5b).

369 The general agreement between the three approaches to estimating absorbing aerosol
 370 influences on 21st century precipitation changes from ScenarioMIP simulations provides
 371 confidence that aerosol cleanup policies can lead to global precipitation rate increases
 372 in excess of 0.5 W m^{-2} ($\approx 0.6\%$ increases on present day rates). Although this is rela-
 373 tively modest when compared with precipitation increases projected for the higher ra-
 374 diative forcings (e.g., $\sim 6\%$ in SSP5-8.5 by the end of the century), if policies for CO₂
 375 mitigation are more aggressive, then absorbing aerosol cleanup will constitute a much
 376 stronger contribution to precipitation increases in the coming century.

377 6 Summary

378 We use data from the ScenarioMIP suite of CMIP6 model simulations to explore
 379 the influence of absorbing aerosols on precipitation changes for four scenarios over the
 380 21st century. Atmospheric energy and water budgets are used to examine influences of
 381 different controls on precipitation, both globally and regionally, between 2015-2025 and
 382 2090-2100. As expected, precipitation increases of $2-3\% \text{ K}^{-1}$ (Fig. 1) are typical because
 383 atmospheric radiative cooling is unable to keep pace with water vapor increases, which
 384 follow Clausius-Clapeyron. Precipitation increases are greater for scenarios with strong
 385 21st century aerosol cleanup. We use a regression approach to isolate the temperature-
 386 independent effects of absorbing aerosol on the shortwave energy budget from the temperature-
 387 dependent effects of water vapor. We show that the apparent global hydrologic sensi-
 388 tivity is 40% stronger in SSP2-4.5 (aerosol cleanup) than in SSP3-7.0 (no cleanup), and
 389 this can be explained primarily by reduced 21st century SW absorption by aerosol in the
 390 former scenario (Fig. 2).

391 This absorbing aerosol influence is found to significantly affect precipitation at the
 392 regional scale (Fig. 3). Two regions are examined, Equatorial Africa ($15^{\circ}\text{S}-15^{\circ}\text{N}, 30^{\circ}\text{W}-$
 393 30°E) and Southeast Asia ($0-45^{\circ}\text{N}, 60-130^{\circ}\text{E}$), both of which experience aerosol cleanup
 394 during SSP2-4.5 but have differing aerosol emissions in SSP3-7.0. The influence of aerosol
 395 cleanup on precipitation via atmospheric shortwave absorption is estimated to be larger
 396 than the impacts of circulation changes in both regions (Fig. 4).

397 The influence of absorbing aerosols on precipitation through the fast, temperature-
 398 independent response is quantified for all ScenarioMIP projections using both the hy-
 399 drologic sensitivity and a multiple linear regression against ΔT and ΔAOD (Fig. 5).
 400 Estimates are consistent with atmospheric energy budget estimations of *AOD* influ-
 401 ence, suggesting absorbing aerosol cleanup policies are likely to boost global precipita-
 402 tion responses by at least 0.5 W m^{-2} ($\approx 0.6\%$ of the present-day global mean rate). For
 403 scenarios with aggressive greenhouse gas mitigation (lower forcing, i.e., SSP1-2.6 and SSP2-
 404 4.5), the aerosol-driven increases in precipitation can significantly contribute to the in-
 405 creases expected from climate warming through the fast-response. This study highlights
 406 the importance of considering aerosol emissions in future policy decisions as those choices
 407 will have critical and long-lasting impacts on both global and regional precipitation and,
 408 as a result, water availability in the future.

409 Acknowledgments

410 We thank Angeline Pendergrass and Dargan Frierson for helpful discussions of this work.
 411 We also acknowledge the World Climate Research Programme and its Working Group
 412 on Coupled Modelling for coordinating CMIP6; the climate modeling groups involved
 413 for their simulations; the Earth System Grid Federation (ESGF) for archiving and fa-
 414 cilitating data usage; and the multiple funding agencies who support CMIP and ESGF
 415 efforts. Research by ILM is supported by the NOAA Climate and Global Change Post-
 416 doctoral Fellowship Program, administered by UCAR's Cooperative Programs for the
 417 Advancement of Earth System Science (CPAESS) under award NA18NWS4620043B. MV
 418 was funded on indirect cost recovery support from grants to UW.

419 Data Availability: All CMIP6 ScenarioMIP simulations used in this study are available
 420 at <https://esgf-node.llnl.gov/projects/cmip6/>.

421 References

- Allan, R. P., Barlow, M., Byrne, M. P., Cherchi, A., Douville, H., Fowler, H. J., ...
 423 Zolina, O. (2020). Advances in understanding large-scale responses of the
 424 water cycle to climate change [Journal Article]. *Ann N Y Acad Sci*, 1472(1),
 425 49–75. Retrieved from <https://www.ncbi.nlm.nih.gov/pubmed/32246848>
 426 doi: 10.1111/nyas.14337
- Allan, R. P., Liu, C., Zahn, M., Lavers, D. A., Koukouvgias, E., & Bodas-Salcedo,
 427 A. (2014, May). Physically Consistent Responses of the Global Atmospheric
 428 Hydrological Cycle in Models and Observations. *Surveys in Geophysics*,
 429 35(3), 533–552. Retrieved 2021-08-24, from <https://doi.org/10.1007/s10712-012-9213-z>
 430 doi: 10.1007/s10712-012-9213-z
- Allen, M. R., & Ingram, W. J. (2002). Constraints on future changes in climate and
 433 the hydrologic cycle [Journal Article]. *Nature*, 419(6903), 228–232. Retrieved
 434 from <https://doi.org/10.1038/nature01092>
- 435 doi: 10.1038/nature01092a.pdf
- Allen, R. J., Evan, A. T., & Booth, B. B. B. (2015). Interhemispheric aerosol
 437 radiative forcing and tropical precipitation shifts during the late twentieth
 438 century [Journal Article]. *Journal of Climate*, 28(20), 8219–8246. Retrieved
 439 from <https://journals.ametsoc.org/view/journals/clim/28/20/jcli-d-15-0148.1.xml>
 440 doi: 10.1175/jcli-d-15-0148.1
- Andrews, T., Forster, P. M., Boucher, O., Bellouin, N., & Jones, A. (2010). Precipitation,
 442 radiative forcing and global temperature change. *Geophysical
 443 Research Letters*, 37(14). Retrieved 2020-09-04, from <https://agupubs.onlinelibrary.wiley.com/doi/abs/10.1029/2010GL043991> (eprint:
 444 <https://agupubs.onlinelibrary.wiley.com/doi/pdf/10.1029/2010GL043991>) doi:
 445 10.1029/2010GL043991
- Bollasina, M. A., Ming, Y., & Ramaswamy, V. (2011). Anthropogenic aerosols and
 447 the weakening of the south asian summer monsoon [Journal Article]. *Science*,
 448 334(6055), 502–505. Retrieved from <https://www.science.org/doi/abs/10.1126/science.1204994>
 450 doi: doi:10.1126/science.1204994
- Chemke, R., & Dagan, G. (2018). The effects of the spatial distribution of direct
 452 anthropogenic aerosols radiative forcing on atmospheric circulation [Journal
 453 Article]. *Journal of Climate*, 31(17), 7129–7145. Retrieved from <https://journals.ametsoc.org/view/journals/clim/31/17/jcli-d-17-0694.1.xml>
 454 doi: 10.1175/jcli-d-17-0694.1
- Dagan, G., & Stier, P. (2020). Constraint on precipitation response to climate
 457 change by combination of atmospheric energy and water budgets [Journal Article].
 458 *npj Climate and Atmospheric Science*, 3(1). doi:
 459 10.1038/s41612-020-00137-8
- Dagan, G., Stier, P., & Watson-Parris, D. (2019a). Analysis of the atmospheric
 461 water budget for elucidating the spatial scale of precipitation changes under
 462 climate change [Journal Article]. *Geophys Res Lett*, 46(17–18), 10504–10511.
 463 Retrieved from <https://www.ncbi.nlm.nih.gov/pubmed/31762521> doi:
 464 10.1029/2019GL084173
- Dagan, G., Stier, P., & Watson-Parris, D. (2019b). Contrasting response of precipitation
 466 to aerosol perturbation in the tropics and extratropics explained by energy
 467 budget considerations [Journal Article]. *Geophys Res Lett*, 46(13), 7828–
 468 7837. Retrieved from <https://www.ncbi.nlm.nih.gov/pubmed/31598021>
 469 doi: 10.1029/2019GL083479
- Dagan, G., Stier, P., & Watson-Parris, D. (2021). An Energetic View
 471 on the Geographical Dependence of the Fast Aerosol Radiative Ef-

- 472 fects on Precipitation. *Journal of Geophysical Research: Atmospheres*,
473 126(9), e2020JD033045. Retrieved 2021-05-28, from <https://agupubs.onlinelibrary.wiley.com/doi/abs/10.1029/2020JD033045> (.eprint:
474 <https://agupubs.onlinelibrary.wiley.com/doi/pdf/10.1029/2020JD033045>) doi:
475 <https://doi.org/10.1029/2020JD033045>

476 DeAngelis, A. M., Qu, X., Zelinka, M. D., & Hall, A. (2015, December). An ob-
477 servational radiative constraint on hydrologic cycle intensification. *Nature*,
478 528(7581), 249–253. Retrieved 2020-05-22, from <https://www.nature.com/articles/nature15770> (Number: 7581 Publisher: Nature Publishing Group)
479 doi: 10.1038/nature15770

480 Eyring, V., Bony, S., Meehl, G. A., Senior, C. A., Stevens, B., Stouffer, R. J.,
481 & Taylor, K. E. (2016, May). Overview of the Coupled Model Inter-
482 comparison Project Phase 6 (CMIP6) experimental design and organiza-
483 tion. *Geoscientific Model Development*, 9(5), 1937–1958. Retrieved 2019-
484 11-15, from <https://www.geosci-model-dev.net/9/1937/2016/> doi:
485 10.5194/gmd-9-1937-2016

486 Held, I. M., & Soden, B. J. (2006). Robust responses of the hydrological cycle to
487 global warming [Journal Article]. *Journal of Climate*, 19(21), 5686–5699. Re-
488 tried from <https://journals.ametsoc.org/view/journals/clim/19/21/jcli3990.1.xml> doi: 10.1175/jcli3990.1

489 Laakso, A., Snyder, P. K., Liess, S., Partanen, A.-I., & Millet, D. B. (2020,
490 May). Differing precipitation response between solar radiation man-
491 agement and carbon dioxide removal due to fast and slow components.
492 *Earth System Dynamics*, 11(2), 415–434. Retrieved 2021-12-22, from
493 <https://esd.copernicus.org/articles/11/415/2020/> (Publisher: Coperni-
494 cus GmbH) doi: 10.5194/esd-11-415-2020

495 Lacis, A. A., & Hansen, J. (1974, January). A Parameterization for the
496 Absorption of Solar Radiation in the Earth's Atmosphere. *Journal
497 of the Atmospheric Sciences*, 31(1), 118–133. Retrieved 2021-12-22,
498 from https://journals.ametsoc.org/view/journals/atsc/31/1/1520-0469_1974_031_0118_apftao_2_0_co_2.xml (Publisher: American
499 Meteorological Society Section: Journal of the Atmospheric Sciences) doi:
500 10.1175/1520-0469(1974)031<0118:APFTAO>2.0.CO;2

501 Lund, M. T., Myhre, G., & Samset, B. H. (2019, November). Anthropogenic
502 aerosol forcing under the Shared Socioeconomic Pathways. *Atmospheric
503 Chemistry and Physics*, 19(22), 13827–13839. Retrieved 2020-05-22, from
504 <https://www.atmos-chem-phys.net/19/13827/2019/> (Publisher: Coperni-
505 cus GmbH) doi: <https://doi.org/10.5194/acp-19-13827-2019>

506 Meinshausen, M., Nicholls, Z. R. J., Lewis, J., Gidden, M. J., Vogel, E., Fre-
507 und, M., ... Wang, R. H. J. (2020). The shared socio-economic pathway
508 (ssp) greenhouse gas concentrations and their extensions to 2500 [Jour-
509 nal Article]. *Geoscientific Model Development*, 13(8), 3571–3605. doi:
510 10.5194/gmd-13-3571-2020

511 Myhre, G., Samset, B. H., Schulz, M., Balkanski, Y., Bauer, S., Berntsen, T. K., ...
512 Zhou, C. (2013). Radiative forcing of the direct aerosol effect from aerocon-
513 phase ii simulations [Journal Article]. *Atmospheric Chemistry and Physics*,
514 13(4), 1853–1877. doi: 10.5194/acp-13-1853-2013

515 Neill, B. C., Tebaldi, C., van Vuuren, D. P., Eyring, V., Friedlingstein, P., Hurtt,
516 G., ... Sanderson, B. M. (2016). The scenario model intercomparison project
517 (scenariomip) for cmip6 [Journal Article]. *Geoscientific Model Development*,
518 9(9), 3461–3482. doi: 10.5194/gmd-9-3461-2016

519 Pendergrass, A. G. (2020). The global-mean precipitation response to co 2 -induced
520 warming in cmip6 models [Journal Article]. *Geophysical Research Letters*,
521 47(17). doi: 10.1029/2020gl089964

522 Pendergrass, A. G., & Hartmann, D. L. (2012). Global-mean pre-

- 527 cipitation and black carbon in AR4 simulations. *Geophysical Re-*
 528 *search Letters*, 39(1). Retrieved 2020-05-22, from <https://agupubs.onlinelibrary.wiley.com/doi/abs/10.1029/2011GL050067> (.eprint:
 529 <https://agupubs.onlinelibrary.wiley.com/doi/pdf/10.1029/2011GL050067>) doi:
 530 10.1029/2011GL050067
- 531 Pendergrass, A. G., & Hartmann, D. L. (2014). The atmospheric energy constraint
 532 on global-mean precipitation change [Journal Article]. *Journal of Climate*,
 533 27(2), 757-768. doi: 10.1175/jcli-d-13-00163.1
- 534 Riahi, K., van Vuuren, D. P., Kriegler, E., Edmonds, J., O'Neill, B. C., Fujii-
 535 mori, S., ... Tavoni, M. (2017). The shared socioeconomic pathways
 536 and their energy, land use, and greenhouse gas emissions implications: An
 537 overview [Journal Article]. *Global Environmental Change*, 42, 153-168. doi:
 538 10.1016/j.gloenvcha.2016.05.009
- 539 Richardson, T. B., Forster, P. M., Andrews, T., Boucher, O., Faluvegi, G.,
 540 Fläschner, D., ... Voulgarakis, A. (2018). Drivers of precipitation change:
 541 An energetic understanding [Journal Article]. *Journal of Climate*, 31(23),
 542 9641-9657. doi: 10.1175/jcli-d-17-0240.1
- 543 Samset, B. H., Myhre, G., Forster, P. M., Hodnebrog, , Andrews, T., Boucher,
 544 O., ... Voulgarakis, A. (2018, January). Weak hydrological sensitiv-
 545 ity to temperature change over land, independent of climate forcing. *npj*
 546 *Climate and Atmospheric Science*, 1(1), 1-8. Retrieved 2021-07-16, from
 547 <https://www.nature.com/articles/s41612-017-0005-5> (Bandiera_abtest:
 548 a_Cc_license_type: cc_by Cg_type: Nature Research Journals Number: 1 Pri-
 549 mary_atype: Research Publisher: Nature Publishing Group Subject_term:
 550 Climate and Earth system modelling;Projection and prediction Sub-
 551 ject_term_id: climate-and-earth-system-modelling;projection-and-prediction)
 552 doi: 10.1038/s41612-017-0005-5
- 553 Samset, B. H., Myhre, G., Forster, P. M., Hodnebrog, , Andrews, T., Faluvegi, G.,
 554 ... Voulgarakis, A. (2016). Fast and slow precipitation responses to individual
 555 climate forcers: A pdrmip multimodel study [Journal Article]. *Geophysical*
 556 *Research Letters*, 43(6), 2782-2791. doi: 10.1002/2016gl068064
- 557 Turnock, S. T., Allen, R. J., Andrews, M., Bauer, S. E., Deushi, M., Emmons, L.,
 558 ... Zhang, J. (2020, November). Historical and future changes in air pol-
 559 lutants from CMIP6 models. *Atmospheric Chemistry and Physics*, 20(23),
 560 14547-14579. Retrieved 2021-11-16, from <https://acp.copernicus.org/articles/20/14547/2020/> (Publisher: Copernicus GmbH) doi: 10.5194/
 561 acp-20-14547-2020
- 562 Wang, C. (2015). Anthropogenic aerosols and the distribution of past large-scale
 563 precipitation change [Journal Article]. *Geophys Res Lett*, 42(24), 10876-10884.
 564 Retrieved from <https://www.ncbi.nlm.nih.gov/pubmed/27134319> doi: 10
 565 .1002/2015GL066416